JACS
JOURNAL OF THE AMERICAN CHEMICAL SOCIETY
Article
pubs.acs.org/JACS

Efficient Organic Solar Cells with Helical Perylene Diimide Electron Acceptors

Yu Zhong,[‡] M. Tuan Trinh,[‡] Rongsheng Chen,[‡,§] Wei Wang,[‡] Petr P. Khlyabich,[∥] Bharat Kumar,[‡] Qizhi Xu,[‡] Chang-Yong Nam,[⊥] Matthew Y. Sfeir,[⊥] Charles Black,[⊥] Michael L. Steigerwald,[‡] Yueh-Lin Loo,[∥] Shengxiong Xiao,*[,†] Fay Ng,*[,‡] X.-Y. Zhu,*[,‡] and Colin Nuckolls*[,†,‡]

[†] The Education Ministry Key Lab of Resource Chemistry, Shanghai Key Laboratory of Rare Earth Functional Materials, Optoelectronic Nano Materials and Devices Institute, Department of Chemistry, Shanghai Normal University, Shanghai 200234, China

[‡]Department of Chemistry, Columbia University, New York, New York 10027, United States

[§]College of Chemical Engineering and Technology, Wuhan University of Science and Technology, Wuhan 430081, China

[∥]Department of Chemical and Biological Engineering, Princeton University, Princeton, New Jersey 08544, United States

[⊥]Center for Functional Nanomaterials, Brookhaven National Laboratory, Upton, New York 11973, United States

Supporting Information

ABSTRACT: We report an efficiency of 6.1% for a solution-processed non-fullerene solar cell using a helical perylene diimide (PDI) dimer as the electron acceptor. Femtosecond transient absorption spectroscopy revealed both electron and hole transfer processes at the donor–acceptor interfaces, indicating that charge carriers are created from photogenerated excitons in both the electron donor and acceptor phases. Light-intensity-dependent current–voltage measurements suggested different recombination rates under short-circuit and open-circuit conditions.

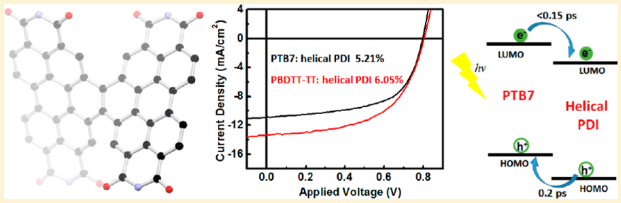

INTRODUCTION

We describe here the device performance, charge transfer dynamics, and recombination mechanisms in a highly efficient fullerene-free organic bulk-heterojunction (BHJ) solar cell. The majority of organic solar cells utilize fullerene and its derivatives ($PC_{61}BM$, $PC_{71}BM$, etc.) as the electron acceptors.[1] Despite their widespread use, fullerene acceptors have some drawbacks. For example, it is difficult to tune the optical properties and electronic structures of fullerenes over a wide range of energy.[2a−c] Furthermore, there are no general methods to enhance the absorption of the fullerene backbone in the visible and NIR regions of the spectrum. Finally, the cost of fullerene derivatives limits their practical use on a large scale.[2d] The acceptor molecule tested here is based on the commercial dye perylene diimide (PDI). PDI and its derivatives have attracted a great deal of attention as alternative electron acceptors because of their good mobility in organic field-effect transistors, high molar absorptivity, ease of functionalization, and economical starting materials. Unfortunately, PDIs and other electron acceptors have not fulfilled their potential in solar cells. Alternatives to fullerenes typically have photon conversion efficiencies (PCEs) in the range of 1−6%.[3−5] Here we present the first solar cells incorporating the helical PDI **1** (Figure 1) as the electron acceptor. We found that solar cells using **1** with either of two commercial donor polymers (Figure 1a) exhibit PCEs greater than 5%. We further characterized these devices by studying their charge carrier recombination processes with incident-light-intensity-dependent performance measurements. Using transient absorption spectroscopy, we demonstrate that excitons generated in both the donor and acceptor phases contribute to the photocurrent by effectively splitting at donor–acceptor interfaces.

RESULTS AND DISCUSSION

Helical PDI **1** is a dimer formed by the fusion of two PDI units with a two-carbon bridge.[6] Figure 1b shows a molecular model of **1**. We recently described a general synthetic route to this material and higher oligomers.[7] Helical **1** has a relatively high electron mobility, good electron-accepting ability, and a LUMO level (~4 eV) similar to those of $PC_{61}BM$ and $PC_{71}BM$.[7] Because of the twisted molecular conformation of **1** (Figure 1b), it does not aggregate strongly.[8] The branched alkyl chains connected to the imide nitrogen atoms ensure good solubility in common organic solvents.[9] **1** absorbs light strongly from 350 to 550 nm with a maximum molar extinction coefficient of 1.1 × 10^5 M^{-1} cm^{-1} (see Figure S1 in the Supporting Information).[6,7] For these reasons and the high molar absorptivity, we decided to test **1** as an electron acceptor in solar cells. To fabricate BHJs based on **1**, we chose the narrow-band-gap semiconducting polymers polythieno[3,4-*b*]-

Received: June 19, 2014
Published: October 14, 2014

   dx.doi.org/10.1021/ja5092613 | J. Am. Chem. Soc. 2014, 136, 15215−15221

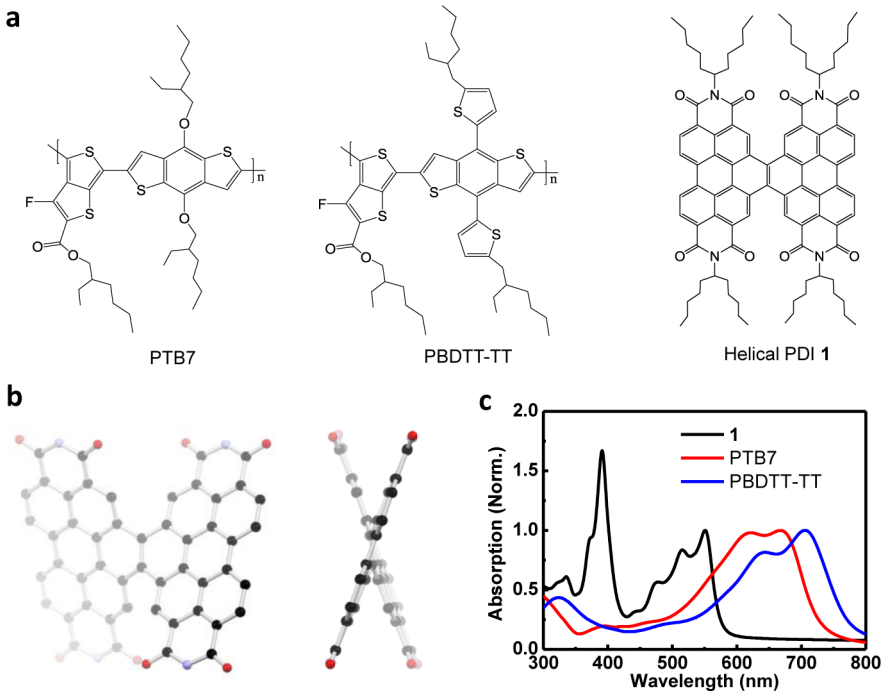

Figure 1. (a) Chemical structures of PTB7, PBDTT-TT, and helical PDI **1**. (b) Molecular model of **1** from DFT calculations. Hydrogens and alkyl side chains have been removed for clarity. Black = carbon; red = oxygen; blue = nitrogen. (c) Film absorption spectra of PTB7, PBDTT-TT, and **1**, normalized at their low-energy λ_{max}.

thiophene-*co*-benzodithiophene (PTB7)[10] and poly[4,8-bis(5-(2-ethylhexyl)thiophen-2-yl)benzo[1,2-*b*;4,5-*b*′]dithiophene-2,6-diyl-*alt*-(4-(2-ethylhexyl)-3-fluorothieno[3,4-*b*]thiophene)-2-carboxylate-2,6-diyl] (PBDTT-TT)[11] (shown in Figure 1a) as the electron donors. The absorption bands of PTB7 and PBDTT-TT are red-shifted relative to those of **1** (Figure 1c); as a result, blended films of **1** and the donor polymers have broad and intense absorptions that span 350 to 800 nm.

We first varied the mass ratio of PTB7 and **1** in solution to optimize the device performance. We fabricated devices in both a conventional structure with a configuration of ITO/PEDOT:PSS(40 nm)/PTB7:**1**/BCP(7 nm)/Al(100 nm) and an inverted structure with a configuration of ITO/ZnO(20 nm)/PTB7:**1**/MoO_x(5 nm)/Al(100 nm). A 3:7 mass ratio of PTB7 and **1** provided the highest PCEs: 3.5% in a conventional structure and 4.5% in an inverted structure. These data are displayed in Figures S2 and S3 in the Supporting Information. Therefore, we chose the inverted structure for further optimization. A schematic of the energy levels in these inverted devices is shown in Figure 2a. Next, we used diiodooctane (DIO) and 1-chloronaphthalene (CN) as solvent additives to improve the overall morphology.[12] Typical current density–voltage (J–V) curves for PTB7:**1** solar cells with different additives are shown in Figure 2b. Compared with devices without additive, those devices with 1% DIO and 1% CN show higher PCEs, mainly because of improvements in the fill factor (FF) from 53.1% without additive to 55.6% with DIO and 54.5% with CN. Furthermore, when 1% DIO and 1% CN were used as coadditives in the solution, the fill factor increased to 60.0%, resulting in an average PCE of 5.14%. The highest PCE we achieved from a PTB7:**1** solar cell is 5.21%. This cell had the following characteristics: short-circuit current density (J_{sc}) = 10.9 mA/cm^2, open-circuit voltage (V_{oc}) = 0.791 V, and FF = 60.0%. We observed a similar effect of DIO and CN with PBDTT-TT:**1** solar cells (Figure 2c). Overall, the solar cells containing PBDTT-TT exhibited larger J_{sc} values than the PTB7 solar cells because of their more red-shifted absorption. The average PCE from six devices without any additives is 5.52%; the average PCEs with various additives are 5.63% with DIO, 5.70% with CN, and 5.94% with DIO and CN as coadditives, respectively. The champion PBDTT-TT:**1** solar cell showed the following characteristics: J_{sc} = 13.3 mA/cm^2, V_{oc} = 0.803 V, FF = 56.6%, and PCE = 6.05%. We summarize the parameters of the solar cells in Table 1. These properties are excellent for a PDI-based solar cell,[4] and the PCEs compete with the highest PCEs reported for solution-processed non-fullerene BHJs.[3,4] These values are lower than those for the corresponding cells with fullerenes as the acceptors,[10,11] but those partners were optimized for each other. This highlights the enormous potential of **1** in solar cells when tailored donor materials are created for them.

We measured the electron and hole mobilities in the optimal blend films by the space-charge-limited current (SCLC) method.[13] For the PTB7:**1** blend film, the hole and electron mobilities were calculated to be 6.7×10^{-5} and 2.2×10^{-4} cm^2 V^{-1} s^{-1}, respectively (Figure S7 in the Supporting Information). This hole mobility is smaller than that of a PTB7:$PC_{71}BM$ blend film,[10a] probably because of the different components and the different mass ratios in the two active layers. For the PBDTT-TT:**1** blend film, the hole and electron mobilities were calculated to be 2.9×10^{-4} and 3.4×10^{-4} cm^2 V^{-1} s^{-1}, respectively. The hole mobility of the PBDTT-TT:**1** blend film is higher than that of PTB7:**1** because of the improved π-stacking of these two-dimensional conjugated polymer chains.[11] In both kinds of devices, helical PDI **1** exhibits electron mobilities 1 order of magnitude higher than those of PTB7:$PC_{71}BM$ and PBDTT-TT:$PC_{71}BM$ BHJs.[11b,14]

Figure 2d displays the external quantum efficiency (EQE) spectra of the optimal PTB7:**1** and PBDTT-TT:**1** devices. Compared with the PTB7:**1** solar cell, the PBDTT-TT:**1** solar

dx.doi.org/10.1021/ja5092613 | J. Am. Chem. Soc. 2014, 136, 15215–15221

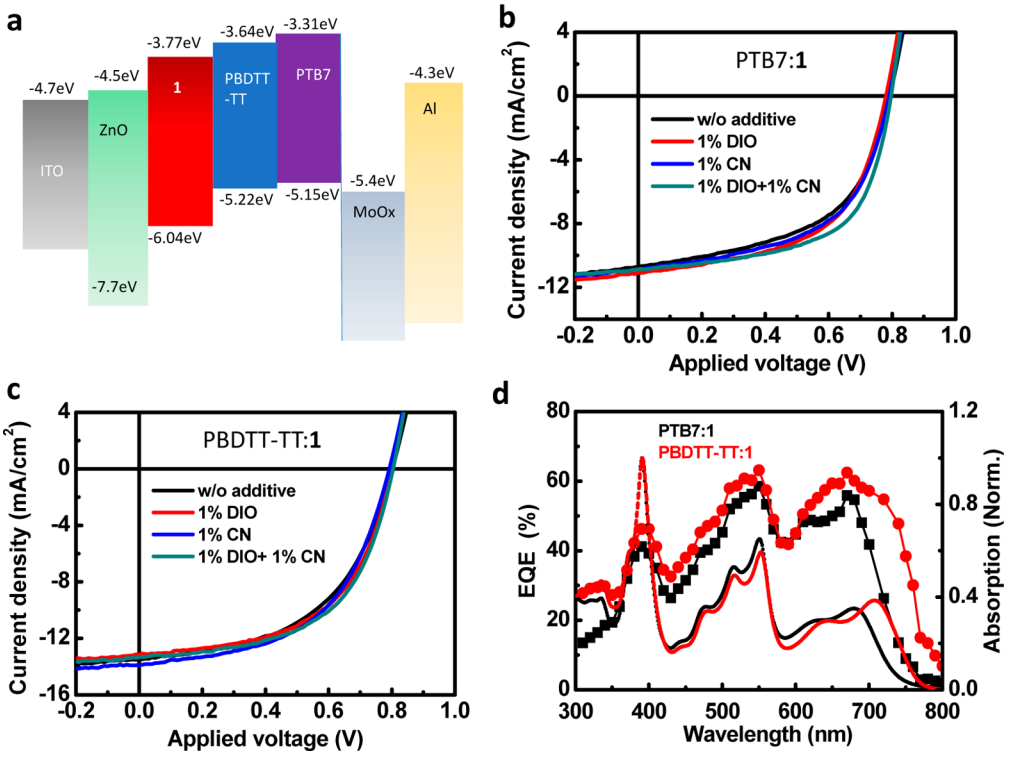

Figure 2. (a) Schematic of the energy levels of ITO, ZnO, **1**, PBDTT-TT, PTB7, MoO_x and Al. (b) J-V curves for PTB7:**1** solar cells with different additives. (c) J-V curves for PBDTT-TT:**1** solar cells with different additives. (d) EQE spectra (symbols) of PTB7: **1** (black) and PBDTT-TT:**1** (red) devices with 1% DIO and 1% CN solvent additive and absorption spectra (dashed lines) for the PTB7:**1** (black) and PBDTT-TT:**1** (red) blend films (3:7 D/A mass ratio).

Table 1. Summary of Device Parameters of PTB7:1 and PBDTT-TT:1 Solar Cells

	J_{sc} (mA/cm^2)	V_{oc} (V)	FF (%)	PCE (%)[a]
PTB7:**1** with no additive	10.5 ± 0.2	0.796 ± 0.006	53.6 ± 0.5	4.47 ± 0.03 (4.50)
PTB7:**1** with 1% DIO	10.9 ± 0.2	0.782 ± 0.004	56 ± 1	4.74 ± 0.05 (4.81)
PTB7:**1** with 1% CN	10.7 ± 0.4	0.787 ± 0.009	54.1 ± 0.8	4.54 ± 0.18 (4.70)
PTB7:**1** with 1% DIO + 1% CN	11.0 ± 0.1	0.789 ± 0.005	59 ± 1	5.14 ± 0.04 (5.21)
PBDTT-TT:**1** with no additive	13.6 ± 0.1	0.796 ± 0.005	51.1 ± 0.7	5.52 ± 0.05 (5.59)
PBDTT-TT:**1** with 1% DIO	13.2 ± 0.1	0.794 ± 0.005	54 ± 1	5.63 ± 0.11 (5.81)
PBDTT-TT:**1** with 1% CN	13.7 ± 0.2	0.790 ± 0.005	53 ± 1	5.70 ± 0.11 (5.86)
PBDTT-TT:**1** with 1% DIO + 1% CN	13.5 ± 0.2	0.796 ± 0.005	55 ± 1	5.94 ± 0.07 (6.05)

[a]Average PCE values were calculated from six devices for each condition; the highest PCE values are shown in parentheses.

cell shows slightly higher EQE values in the range of 300 to 700 nm and a significant increase from 700 to 800 nm due to the red-shifted absorption of PBDTT-TT. The integrated J_{sc} values are 10.2 mA/cm^2 for the PTB7:**1** solar cell and 12.8 mA/cm^2 for PBDTT-TT:**1** solar cell, giving estimated PCEs of 4.9% for the former and 5.8% for the latter. These values agree well with the PCEs in Table 1, and it should be noted that the EQE values are not zero at 300 nm, resulting in a slight underestimation of the PCEs when the EQE spectra are used. Unlike those solar cells made from fullerene derivatives and other non-fullerene acceptors, both of the EQE curves show three transitions instead of a featureless transition. These peaks arise from the sharp and strong absorption bands of **1** (Figure 1c). This feature is unique among PDI-based non-fullerene BHJs because **1** has a rigid conformation that is different from those of other PDI acceptors.[4] The important point is that we are able to distinguish the photoresponse peaks of the donor polymers and that of **1**. We note that the shape of the EQE spectrum is similar to the absorption spectrum of the blend film. Since the absorption from 350 to 550 nm for the blend film is mainly from **1**, photogenerated excitons from **1** largely contribute to the photocurrent in these solar cells.

A particular advantage of helical PDI **1** over fullerenes as the electron acceptor is the higher optical absorption cross section of the former. To unambiguously establish that light absorption in both the donor and acceptor contribute to the photocurrent in a **1**-based BHJ and to establish the charge generation mechanisms, we used transient absorption (TA) spectroscopy. Figure 3 shows the differential transmission spectra and dynamics for a film of neat **1** excited at 390 nm. The negative features with peaks at 480, 516, and 556 nm (Figure 3a) result from bleaching of the ground-state absorption as charges and excitons are created in **1**. The positive signals in the wavelength ranges below 470 nm and above 570 nm are the excited-state absorption (ESA) of the photogenerated charges or excitons in the film. The ESA feature for the film of **1** centered at 700 nm can be assigned to the singlet $S_1 \rightarrow S_N$ transitions.[15] It decays

dx.doi.org/10.1021/ja5092613 | J. Am. Chem. Soc. 2014, 136, 15215−15221

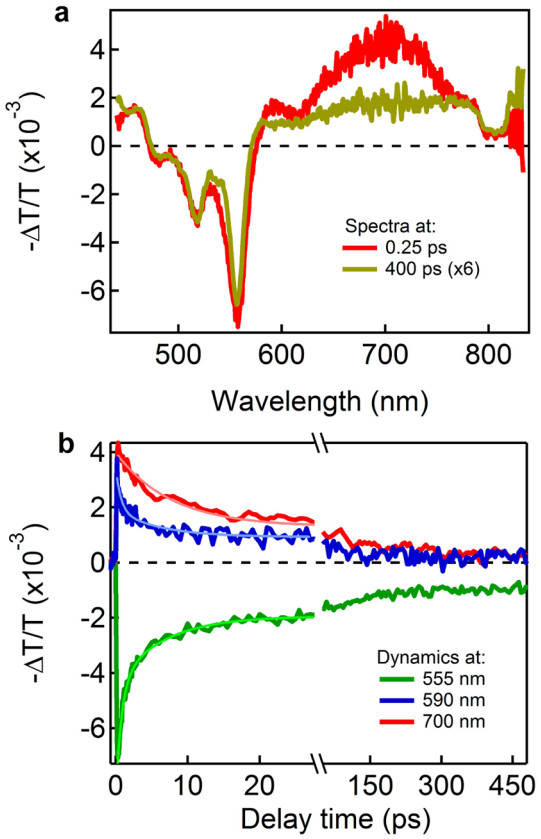

Figure 3. (a) Differential transmission spectra ($-\Delta T/T$) as a function of probe wavelength with pumping at 390 nm for neat **1** at 0.25 and 400 ps. The excited-state absorption (ESA) centered at 700 nm at 0.25 ps is due to $S_1 \rightarrow S_N$ transitions. The dip at 800 nm is due to saturation caused by high probe intensity. (b) Dynamics at probe wavelengths of 555, 590, and 700 nm.

with a single-exponential lifetime of τ_{S1} = 8.6 ± 0.4 ps (red curve in Figure 3b).

Unlike the simple S_1 decay, the dynamics of ground-state recovery probed at 555 nm (green curve in Figure 3b) is more complex and can be described by three distinct time constants (triexponential fit in Figure 3b) with relative populations in parentheses: τ_1 = 0.81 ± 0.07 ps (39%), τ_2 = 8.6 ± 0.7 ps (35%), and τ_3 = 800 ± 50 ps (26%). The intermediate component (τ_2 = 8.6 ± 0.7 ps) has a time constant identical to that of the singlet decay and is assigned to S_1. The faster (0.81 ps) and slower (800 ps) components do not correspond to S_1 and must be attributed to different species. Since initial photoexcitation in molecular semiconductors is known to generate both excitons and free charge carriers,[16] we assign the ground-state recovery with τ_1 = 0.81 ± 0.07 ps and τ_3 = 800 ± 50 ps to the recombination of charge carriers: the faster component to geminate recombination of the nascent electron−hole pairs and the slower one to two-body recombination of individual electron and hole carriers (bimolecular recombination). Evidence for the generation of photocarriers can also be found in the ESA. The fast ESA feature at 590 nm with a decay time constant of 0.7 ± 0.1 ps (blue curve in Figure 3b) is very close to the fast decay component of bleaching recovery and thus is assigned to geminate recombination. There is a broad ESA feature in the TA spectrum at 400 ps spanning from 580 to 850 nm (Figure 3a). This recovery occurs on the 800 ps time scale and can be assigned to bimolecular recombination of the individual electron and hole carriers (Figure 3a).[16b,c] From the above fit to the bleaching dynamics at 555 nm, we assign a direct charge generation yield of 26% in the film of **1** upon photoexcitation. It should be noted that we do not assign the slow component to triplets because the triplet absorption in PDI derivatives is known to give a sharp feature in the wavelength region below 600 nm.[15c,17] These features are absent in the TA spectrum (green-yellow curve in Figure 3a).

Having investigated the photophysics in neat **1**, we next explored the exciton generation and dissociation in a blend of **1** and PTB7 at a mass ratio of 3:7. Figure 4a shows the differential transmission spectra for three films: neat **1**, neat PTB7, and a blend of PTB7 and **1**. At a pump wavelength of 670 nm, we excite only PTB7, not **1** (red solid curve). The black dashed curve represents the TA spectrum for neat PTB7 at a probe delay of 0.25 ps. The negative features with maxima at 625 and 680 nm result from bleaching of the ground-state absorption as excitons are created in PTB7. The TA spectrum for the blended film at the same excitation wavelength shows, in addition to ground-state bleaching of PTB7, new features at 515 and 555 nm that we attribute to ground-state bleaching of PDI. The TA spectrum of neat **1** excited at 390 nm (the red dashed curve in Figure 4b is reproduced from Figure 3a) verifies this assignment. The appearance of ground-state bleaching of **1** when only PTB7 is photoexcited in the blend is evidence of charge (electron) transfer from the photoexcited donor, PTB7, to the electron acceptor, **1**.

Similar results on photoinduced charge transfer were obtained when we preferentially excited **1** in the blend at 390 nm. At this wavelength, most of the incident light is absorbed by **1**, but a small fraction of the light is also absorbed by PTB7 (see the absorption spectra in Figure 1c). As shown in Figure 4b, the spectra at a short time (0.25 ps) show ground-state bleaching for both PTB7 and **1**. At longer times (6 ps) the bleaching signal in the wavelength range from 600 to 720 nm increases, indicating more charge (hole) transfer from **1** into PTB7.

In addition to ground-state bleaching and excitonic peaks assigned to PTB7 and **1**, we also observe a broad and strong induced-absorption feature that is most evident at >700 nm (Figure 4a,b), where overlap with the ground-state bleaching and ESA are at a minimum. For pumping at 670 nm, the carriers are generated only in the blend, not in neat PTB7 or **1**. At the shorter excitation wavelength of 390 nm, we observe photocarrier generation in both the blend and neat PTB7 or **1**, with the amount of photocarrier generation enhanced being in the blend films.

With the above assignment of photophysical processes, we now turn to their dynamics. We present the time evolution of the photobleaching and induced-absorption features from the blended film in Figure 4c,d for photoexcitation at 670 and 390 nm, respectively. Upon excitation of only PTB7 in the blend (at 670 nm), the induced absorption at 785 nm rises very fast (within the experimental resolution, <150 fs), indicating ultrafast electron transfer from PTB7 to **1**. This time scale is consistent with the ultrafast electron transfer in other reported heterojunctions of conjugated polymers with fullerenes.[18] In addition to the ultrafast rise, there is a slower rise that is 23% of the total induced absorption amplitude with a time constant of 0.4 ps. We attribute this slower rise to exciton diffusion in PTB7 toward interfaces prior to exciton dissociation.[19] The recovery of PTB7 ground-state bleaching probed at 690 nm

dx.doi.org/10.1021/ja5092613 | J. Am. Chem. Soc. 2014, 136, 15215−15221

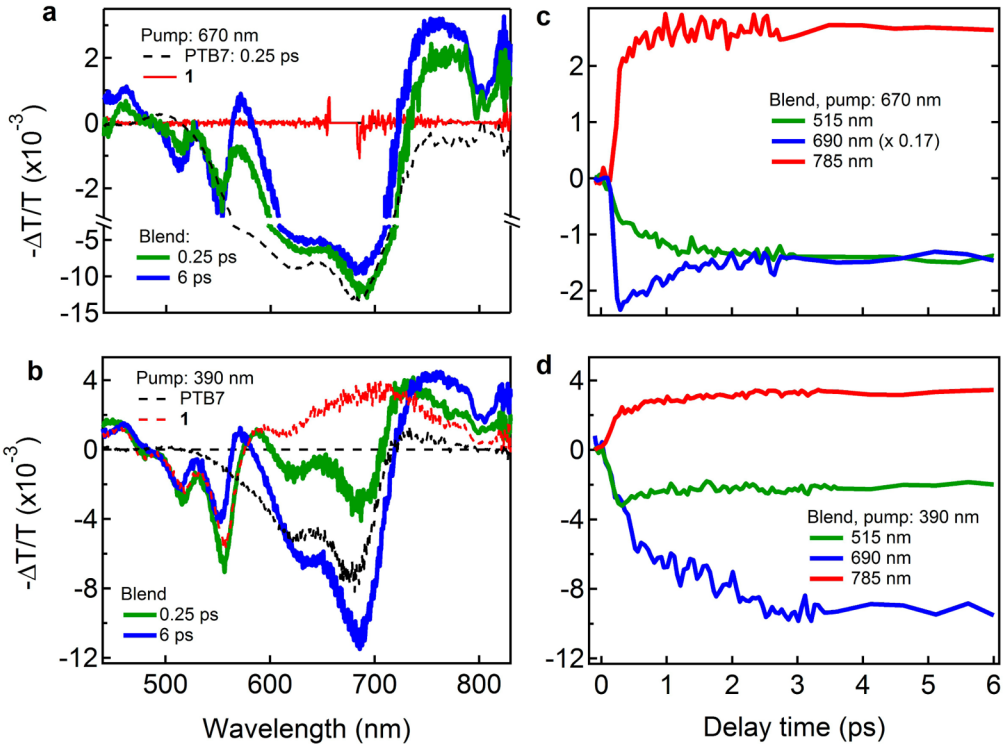

Figure 4. (a, b) Differential transmission spectra ($-\Delta T/T$) as a function of probe wavelength with pumping at (a) 670 nm and (b) 390 nm for neat **1** and neat PTB7 at 0.25 ps and a blend of **1** and PTB7 films at 0.25 and 6 ps. (c, d) Decay dynamics at the different probe wavelengths with pumping at 670 and 390 nm. The dynamics at the probe wavelength of 690 nm in panel (c) has been scaled by a factor of 0.17. The pump density was ~20 μJ/cm^2 per pulse.

(blue curve in Figure 4c) occurs clearly on two very different time scales; the biexponential fit gives a fast decay channel with a time constant of 0.7 ps accounting for 40% of the total bleaching amplitude and a slower one with a time constant of 1 ns accounting for the remaining 60% (see Figure S8 in the Supporting Information). The fast decay is a loss channel via exciton recombination in PTB7. This fast decay is similar to that of neat PTB7 during the first 3 ps. The remaining 60% of photoexcited PTB7 leads to efficient charge separation at the donor–acceptor interface; the charge carriers subsequently undergo bimolecular recombination (on the 1 ns time scale) in the absence of charge extraction. This decay time constant is consistent with the decay dynamics of excited-state absorption probed at 785 nm (Figure S8), which we attribute to charge carriers. Similar to that of charge-induced absorption at 785 nm, the bleaching signal of **1** at 515 nm (green curve in Figure 4c) consists of two components resulting from the ultrafast interfacial electron transfer and exciton diffusion. This bleaching signal also recovers on the ~1 ns time scale attributed to bimolecular recombination.

When both **1** and PTB7 are excited in the blend at 390 nm, the PTB7 ground-state bleaching probed at 690 nm (blue curve in Figure 4d) consists of two components: an initial fast rise and a slower rise with time constants of 0.2 and 1.2 ps, respectively. The former, with an amplitude of 62%, is attributed to direct photoexcitation of PTB7 and hole transfer from **1** into PTB7, while the latter, with an amplitude of 38%, is due to exciton diffusion in **1** toward interfaces prior to the exciton dissociation. At 390 nm excitation, the recovery of the bleaching signal at 690 nm and the decay dynamics of excited-state absorption probed at 785 nm are ~1 ns, consistent with charge recombination when pumped at 670 nm (Figure S8).

On the basis of the transient absorption results presented above, we conclude that electron and hole transfer from the photoexcited donor and acceptor, respectively, both occur efficiently at the donor–acceptor interfaces in the blended film. Scheme 1 summarizes the competition among the different channels.

Scheme 1. Summary of the Exciton Generation and Charge Separation in the Blend of 1 and PTB7 at High Excitation Energy[a]

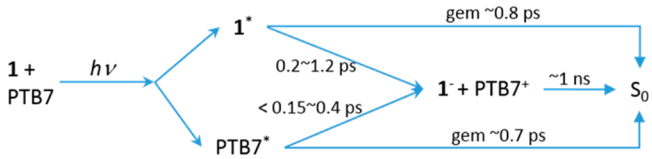

[a]The * labels denote the exciton, and the − and + labels denote molecules with positive and negative charges, respectively.

The transient absorption measurements presented above reveal bimolecular recombination of charge carriers in the blend film in the absence of charge extraction. To establish the relative importance of the recombination channels in the solar cell configuration, we measured the J–V characteristics of our devices as a function of incident light intensity from 1 to 100 mW/cm^2.[20] Figure S9 in the Supporting Information displays the J–V curves for a typical optimized PTB7:**1** solar cell under different incident light intensities. We extracted J_{sc} and V_{oc} values from each curve to evaluate the recombination processes under short-circuit and open-circuit conditions, respectively. Figure 5a shows a log–log plot of J_{sc} as a function of light intensity. By fitting the curve to the power-law dependence of

dx.doi.org/10.1021/ja5092613 | J. Am. Chem. Soc. 2014, 136, 15215–15221

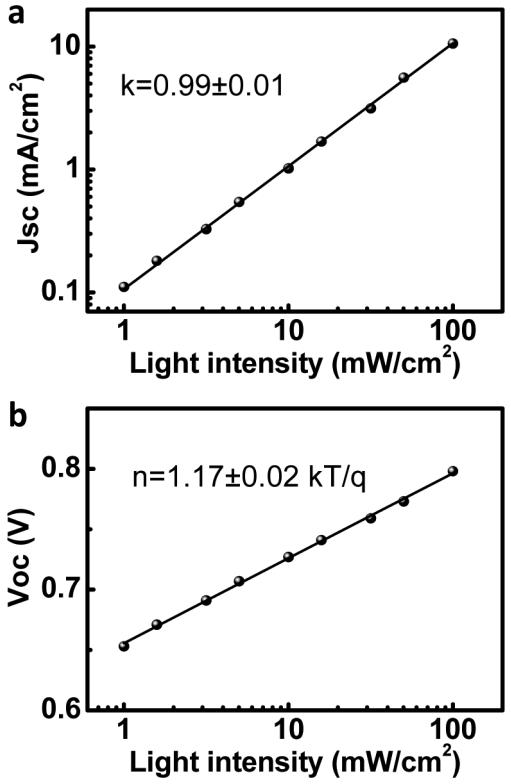

Figure 5. (a) Log–log plot of J_{sc} as a function of light intensity and (b) semilogarithmic plot of V_{oc} as a function of light intensity for an optimized PTB7:**1** device.

J_{sc} on light intensity, expressed as $J_{sc} \propto I^{\alpha}$, we determined the value of α to be 0.99 ± 0.01. This near-unity exponent indicates that monomolecular recombination is active.[20b] The bimolecular recombination or space-charge effects are very weak under short-circuit conditions.[21] The semilogarithmic plot of V_{oc} as a function of light intensity is shown in Figure 5b. We fitted the experimental data to give the slope of V_{oc} versus the natural logarithm of the light intensity. From 100 mW/cm^2 (1 sun) to 1 mW/cm^2 (0.01 sun), the slope was calculated to be $(1.17 \pm 0.02)kT/q$, suggesting that recombination is a combination of monomolecular and bimolecular processes.[20b] The same experiment carried out on the PBDTT-TT:**1** solar cell gave similar results (Figure S10 in the Supporting Information). The extracted slopes for log J_{sc} versus log I and V_{oc} versus log I are 0.96 ± 0.01 and $(1.20 \pm 0.03)kT/q$, respectively (Figure S11 in the Supporting Information). We note that these experimental results are very similar to those for classical P3HT:PCBM solar cells,[20b] indicating that the same level of recombination loss may account for the high performance of our solar cells. More recently, Zang et al.[4g] reported a highly efficient non-fullerene solar cell, but the specific types of monomolecular recombination that occur in these cells are unknown. Sharenko and coworkers proposed trap-dominant device performance in a PDI-monomer-based solar cell.[4b] However, geminate recombination may also contribute to the charge carrier loss, as proposed for the PTB7:fullerene solar cell[22] and PDI-based solar cells.[4b]

CONCLUSION

We have reported a solution-processed organic solar cell based on the combination of the helical electron-accepting PDI **1** and commercially available electron-donating PTB7 and PBDTT-TT. These solar cells show photon conversion efficiencies that are among the highest reported for non-fullerene-based solar cells.[3−5] We have demonstrated exciton generation in both the donor and acceptor materials. Transient absorption spectroscopy revealed ultrafast electron transfer from PTB7 to **1** and hole transfer from **1** to PTB7 with a time constant of ∼0.2 ps. Incident-light-intensity-dependent measurements suggested different recombination mechanisms under open-circuit and short-circuit conditions. By fine-tuning the molecular structure of the PDI dimer, we will be able to further improve the performance of these materials in solar cells.

ASSOCIATED CONTENT

Supporting Information

Device fabrication, characterization methods, absorption spectra, device performance, AFM images, carrier mobility measurements, femtosecond transient absorption measurements, and incident-light-intensity-dependent measurements. This material is available free of charge via the Internet at http://pubs.acs.org.

AUTHOR INFORMATION

Corresponding Authors

senksong@msn.com
fwn2@columbia.edu
xz2324@columbia.edu
cn37@columbia.edu

Notes

The authors declare no competing financial interest.

ACKNOWLEDGMENTS

Support for this project was provided by the Chemical Sciences, Geosciences and Biosciences Division, Office of Basic Energy Sciences, U.S. Department of Energy (DOE) under Award DE-FG02-01ER15264. S.X. thanks the Shanghai Municipal Science and Technology Commission (12nm0504000), the Program for Professor of Special Appointment (Eastern Scholar) at Shanghai Institutions of Higher Learning (2013-57), the Program for Changjiang Scholars and Innovative Research Team in University (IRT1269), the International Joint Laboratory on Resource Chemistry (IJLRC), and the National Natural Science Foundation of China (21473113). M.T.T. and X.-Y.Z. were supported by the U.S. National Science Foundation (Grant DMR 1321405). Portions of the research were carried out at the Center for Functional Nanomaterials at Brookhaven National Laboratory, supported by the U.S. Department of Energy, Office of Basic Energy Sciences, under Contract DE-AC02-98CH10886. R.C. thanks the National Natural Science Foundation of China (Grant 21105077) for support. Portions of this work were supported as part of the program "Center for Re-Defining Photovoltaic Efficiency through Molecule Scale Control", an Energy Frontier Research Center funded by the U.S. Department of Energy, Office of Science, Office of Basic Energy Sciences under Award DE-SC0001085.

REFERENCES

(1) (a) Dou, L.; You, J.; Hong, Z.; Xu, Z.; Li, G.; Street, R. A.; Yang, Y. *Adv. Mater.* **2013**, *25*, 6642−6671. (b) Thompson, B. C.; Fréchet, J. M. J. *Angew. Chem., Int. Ed.* **2008**, *47*, 58−77.

(2) (a) Lenes, M.; Shelton, S. W.; Sieval, A. B.; Kronholm, D. F.; Hummelen, J. C.; Blom, P. W. M. *Adv. Funct. Mater.* **2009**, *19*, 3002−3007. (b) Ross, R. B.; Cardona, C. M.; Guldi, D. M.; Sankaranarayanan, S. G.; Reese, M. O.; Kopidakis, N.; Peet, J.;

Walker, B.; Bazan, G. C.; Van Keuren, E.; Holloway, B. C.; Drees, M. *Nat. Mater.* **2009**, *8*, 208−212. (c) He, Y.; Chen, H.-Y.; Hou, J.; Li, Y. *J. Am. Chem. Soc.* **2010**, *132*, 1377−1382. (d) Anctil, A.; Babbitt, C. W.; Raffaelle, R. P.; Landi, B. J. *Environ. Sci. Technol.* **2011**, *45*, 2353−2359.

(3) For examples of non-fullerene bulk-junction solar cells, see: (a) Woo, C. H.; Holcombe, T. W.; Unruh, D. A.; Sellinger, A.; Fréchet, J. M. J. *Chem. Mater.* **2010**, *22*, 1673−1679. (b) Zhou, Y.; Dai, Y.-Z.; Zheng, Y.-Q.; Wang, X.-Y.; Wang, J.-Y.; Pei, J. *Chem. Commun.* **2013**, *49*, 5802−5804. (c) Winzenberg, K. N.; Kemppinen, P.; Scholes, F. H.; Collis, G. E.; Shu, Y.; Birendra Singh, T.; Bilic, A.; Forsyth, C. M.; Watkins, S. E. *Chem. Commun.* **2013**, *49*, 6307−6309. (d) Ren, G.; Ahmed, E.; Jenekhe, S. A. *J. Mater. Chem.* **2012**, *22*, 24373−24379. (e) Li, H.; Kim, F. S.; Ren, G.; Hollenbeck, E. C.; Subramaniyan, S.; Jenekhe, S. A. *Angew. Chem., Int. Ed.* **2013**, *52*, 5513−5517. (f) Boudreault, P.-L. T.; Michaud, A.; Leclerc, M. *Macromol. Rapid Commun.* **2007**, *28*, 2176−2179. (g) Douglas, J. D.; Chen, M. S.; Niskala, J. R.; Lee, O. P.; Yiu, A. T.; Young, E. P.; Fréchet, J. M. J. *Adv. Mater.* **2014**, *26*, 4313−4319. (h) Eftaiha, A. F.; Sun, J.-P.; Hill, I. G.; Welch, G. C. *J. Mater. Chem. A* **2014**, *2*, 1201−1213.

(4) For examples of non-fullerene solar cells based on PDIs, see: (a) Lin, Y.; Wang, Y.; Wang, J.; Hou, J.; Li, Y.; Zhu, D.; Zhan, X. *Adv. Mater.* **2014**, *26*, 5137−5142. (b) Sharenko, A.; Proctor, C. M.; van der Poll, T. S.; Henson, Z. B.; Nguyen, T.-Q.; Bazan, G. C. *Adv. Mater.* **2013**, *25*, 4403−4406. (c) Zhang, X.; Lu, Z.; Ye, L.; Zhan, C.; Hou, J.; Zhang, S.; Jiang, B.; Zhao, Y.; Huang, J.; Zhang, S.; Liu, Y.; Shi, Q.; Liu, Y.; Yao, J. *Adv. Mater.* **2013**, *25*, 5791−5797. (d) Jiang, W.; Ye, L.; Li, X.; Xiao, C.; Tan, F.; Zhao, W.; Hou, J.; Wang, Z. *Chem. Commun.* **2014**, *50*, 1024−1026. (e) Lu, Z.; Jiang, B.; Zhang, X.; Tang, A.; Chen, L.; Zhan, C.; Yao, J. *Chem. Mater.* **2014**, *26*, 2907−2914. (f) Zhou, Y.; Kurosawa, T.; Ma, W.; Guo, Y.; Fang, L.; Vandewal, K.; Diao, Y.; Wang, C.; Yan, Q.; Reinspach, J.; Mei, J.; Appleton, A. L.; Koleilat, G. I.; Gao, Y.; Mannsfeld, S. C. B.; Salleo, A.; Ade, H.; Zhao, D.; Bao, Z. *Adv. Mater.* **2014**, *26*, 3767−3772. (g) Zang, Y.; Li, C.-Z.; Chueh, C.-C.; Williams, S. T.; Jiang, W.; Wang, Z.-H.; Yu, J.-S.; Jen, A. K. Y. *Adv. Mater.* **2014**, *26*, 5708−5714.

(5) Higher PCE has been achieved in a fullerene-free organic solar cell with a multilayer structure. See: Cnops, K.; Rand, B. P.; Cheyns, D.; Verreet, B.; Empl, M. A.; Heremans, P. *Nat. Commun.* **2014**, *5*, No. 3406.

(6) Li, Y.; Wang, C.; Li, C.; Di Motta, S.; Negri, F.; Wang, Z. *Org. Lett.* **2012**, *14*, 5278−5281.

(7) Zhong, Y.; Kumar, B.; Oh, S.; Trinh, M. T.; Wu, Y.; Elbert, K.; Li, P.; Zhu, X.; Xiao, S.; Ng, F.; Steigerwald, M. L.; Nuckolls, C. *J. Am. Chem. Soc.* **2014**, *136*, 8122−8130.

(8) Strong aggregation is a problem for PDIs in organic BHJs. See: (a) Sharma, G. D.; Suresh, P.; Mikroyannidis, J. A.; Stylianakis, M. M. *J. Mater. Chem.* **2010**, *20*, 561−567. (b) Kamm, V.; Battagliarin, G.; Howard, I. A.; Pisula, W.; Mavrinskiy, A.; Li, C.; Müllen, K.; Laquai, F. *Adv. Energy Mater.* **2011**, *1*, 297−302.

(9) C7-helical PDI has very poor solubility in chloroform and chlorobenzene and cannot form smooth films by the spin-coating process.

(10) (a) Liang, Y.; Xu, Z.; Xia, J.; Tsai, S.-T.; Wu, Y.; Li, G.; Ray, C.; Yu, L. *Adv. Mater.* **2010**, *22*, E135−E138. (b) He, Z. C.; Zhong, C. M.; Su, S. J.; Xu, M.; Wu, H. B.; Cao, Y. *Nat. Photonics* **2012**, *6*, 591−595.

(11) (a) Cui, C.; Wong, W.-Y.; Li, Y. *Energy Environ. Sci.* **2014**, *7*, 2276−2284. (b) Liao, S.-H.; Jhuo, H.-J.; Cheng, Y.-S.; Chen, S.-A. *Adv. Mater.* **2013**, *25*, 4766−4771.

(12) (a) Lee, J. K.; Ma, W. L.; Brabec, C. J.; Yuen, J.; Moon, J. S.; Kim, J. Y.; Lee, K.; Bazan, G. C.; Heeger, A. J. *J. Am. Chem. Soc.* **2008**, *130*, 3619−3623. (b) Graham, K. R.; Wieruszewski, P. M.; Stalder, R.; Hartel, M. J.; Mei, J.; So, F.; Reynolds, J. R. *Adv. Funct. Mater.* **2012**, *22*, 4801−4813. (c) Guo, X.; Cui, C.; Zhang, M.; Huo, L.; Huang, Y.; Hou, J.; Li, Y. *Energy Environ. Sci.* **2012**, *5*, 7943−7949.

(13) Malliaras, G. G.; Salem, J. R.; Brock, P. J.; Scott, C. *Phys. Rev. B* **1998**, *58*, R13411−R13414.

(14) Lee, B. R.; Jung, E. D.; Nam, Y. S.; Jung, M.; Park, J. S.; Lee, S.; Choi, H.; Ko, S.-J.; Shin, N. R.; Kim, Y.-K.; Kim, S. O.; Kim, J. Y.; Shin, H.-J.; Cho, S.; Song, M. H. *Adv. Mater.* **2014**, *26*, 494−500.

(15) (a) Giaimo, J. M.; Lockard, J. V.; Sinks, L. E.; Scott, A. M.; Wilson, T. M.; Wasielewski, M. R. *J. Phys. Chem. A* **2008**, *112*, 2322−2330. (b) Ramanan, C.; Smeigh, A. L.; Anthony, J. E.; Marks, T. J.; Wasielewski, M. R. *J. Am. Chem. Soc.* **2012**, *134*, 386−397. (c) Eaton, S. W.; Shoer, L. E.; Karlen, S. D.; Dyar, S. M.; Margulies, E. A.; Veldkamp, B. S.; Ramanan, C.; Hartzler, D. A.; Savikhin, S.; Marks, T. J.; Wasielewski, M. R. *J. Am. Chem. Soc.* **2013**, *135*, 14701−14712.

(16) (a) Piris, J.; Dykstra, T. E.; Bakulin, A. A.; van Loosdrecht, P. H. M.; Knulst, W.; Trinh, M. T.; Schins, J. M.; Siebbeles, L. D. A. *J. Phys. Chem. C* **2009**, *113*, 14500−14506. (b) Howard, I. A.; Laquai, F.; Keivanidis, P. E.; Friend, R. H.; Greenham, N. C. *J. Phys. Chem. C* **2009**, *113*, 21225−21232. (c) Holman, M. W.; Yan, P.; Adams, D. M.; Westenhoff, S.; Silva, C. *J. Phys. Chem. A* **2005**, *109*, 8548−8552.

(17) Ford, W. E.; Kamat, P. V. *J. Phys. Chem.* **1987**, *91*, 6373−6380.

(18) (a) Hwang, I.; Beaupre, S.; Leclerc, M.; Scholes, G. D. *Chem. Sci.* **2012**, *3*, 2270−2277. (b) Hwang, I. W.; Soci, C.; Moses, D.; Zhu, Z.; Waller, D.; Gaudiana, R.; Brabec, C. J.; Heeger, A. J. *Adv. Mater.* **2007**, *19*, 2307−2312. (c) Grancini, G.; Maiuri, M.; Fazzi, D.; Petrozza, A.; Egelhaaf, H.-J.; Brida, D.; Gerullo, G.; Lanzani, G. *Nat. Mater.* **2013**, *12*, 29−33. (d) Gélinas, S.; Rao, A.; Kumar, A.; Smith, S. L.; Chin, A. W.; Clark, J.; van der Poll, T. S.; Bazan, G. C.; Friend, R. H. *Science.* **2014**, *343*, 512−516.

(19) Kaake, L. G.; Jasieniak, J. J.; Bakus, R. C.; Welch, G. C.; Moses, D.; Bazan, G. C.; Heeger, A. J. *J. Am. Chem. Soc.* **2012**, *134*, 19828−19838.

(20) (a) Koster, L. J. A.; Mihailetchi, V. D.; Ramaker, R.; Blom, P. W. M. *Appl. Phys. Lett.* **2005**, *86*, No. 123509. (b) Cowan, S. R.; Roy, A.; Heeger, A. J. *Phys. Rev. B* **2010**, *82*, No. 245207.

(21) Koster, L. J. A.; Mihailetchi, V. D.; Xie, H.; Blom, P. W. M. *Appl. Phys. Lett.* **2005**, *87*, No. 203502.

(22) Foertig, A.; Kniepert, J.; Gluecker, M.; Brenner, T.; Dyakonov, V.; Neher, D.; Deibel, C. *Adv. Funct. Mater.* **2014**, *24*, 1306−1311.